Journal of Materials Chemistry A

Accepted Manuscript

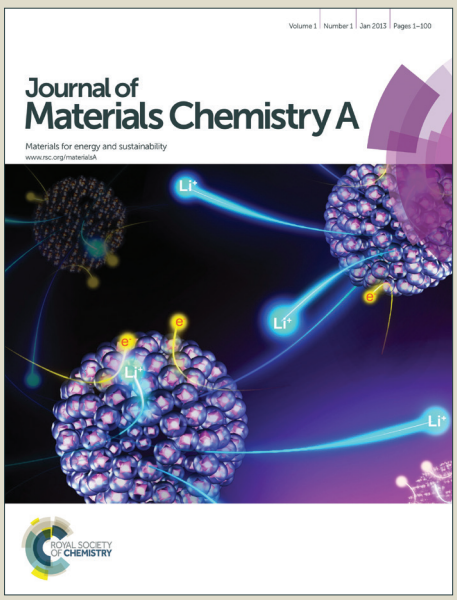

ROYAL SOCIETY OF CHEMISTRY

www.rsc.org/materialsA

Journal of Materials Chemistry A

ARTICLE

Thermoelectric and Electrical Transport Properties of Mg_2Si Multi-doped with Sb Al and Zn

Received 00th January 20xx,
Accepted 00th January 20xx

DOI: 10.1039/x0xx00000x

www.rsc.org/

Jianbao Zhao[a], Zhenxian Liu[b], Joel Reid[c], Kenichi Takarabe[d], Tsutomu Iida[e], Bosen Wang[f], Uwatoko Yoshiya[f] and John S. Tse[a,*]

Enhanced thermoelectric and electrical transport properties of Mg_2Si-based thermoelectric materials have been achieved by multi-doping with Sb Al and Zn. Results on the investigation of the electrical transport and thermoelectric properties of multi-doped samples prepared using the spark plasma sintering technique are reported. Synchrotron radiation powder X-ray diffraction was used to characterize the structures of the doped samples. The electrical transport properties were determined from mid-infrared reflectivities, Hall effect and conventional quasi-four probe conductivity measurements. Using the electron concentrations (*N*) determined from the Hall coefficients, the effective masses (*m**) were calculated from the frequency of the plasma edge (ω_P) of the infrared reflectivities. The thermoelectric performance and thermoelectric figure of merits (ZT) 300 K to 900 K of the doped Mg_2Si compounds were calculated from the measured temperature dependent electrical conductivity (σ), Seebeck coefficient (S), and thermal conductivity (κ). A maximum ZT of 0.964 was found in Sb0.5%Zn0.5% doped Mg_2Si at 880 K. This value is comparable to the PbTe based thermoelectric materials.

Introduction

Doped Magnesium silicide (Mg_2Si)-based alloys have been suggested to be a new generation of high performance and environmental friendly thermoelectric materials.[1-4] Compared to lead-based thermoelectric materials, Mg_2Si-based alloys have the merits of being non-toxic, sustainable and low production cost. The efficiency of thermoelectric materials can be enhanced through *p*- or *n*-type doping.[5-9] Dopants can increase the carrier concentration and mobility of the conduction electrons. Doping with heavy atoms can also affect the lattice vibrations and help to lower the thermal conductivity. It was reported that at the presence of Sb and Bi, Mg_2Si had exhibited good thermoelectric performance.[10] For example, Akasaka *et al.* had found that the figure of merit for Bi-doped and Ag-doped, *n*- and *p*-doping respectively, were 0.65 at 840 K and 0.1 at 566 K.[11]

More recently, *p*-type and *n*-type Mg_2Si thermoelectric materials multi-doped with more than one element have led to further enhancement of the thermoelectric figure of merit. In 2010, $Mg_2Si_{0.25}Sn_{0.75}$ doped with Li and Ag was investigated by Isoda *et al.*[12] Compared to the single-doped samples, in double-doped $Mg_2Si_{0.25}Sn_{0.75}$ with Li (20000 ppm) and Ag (5000 ppm) the Seebeck coefficients have increased and maximized to 250 μVK^{-1} at 500 K. The previous Seebeck coefficients were found to be positive, indicating *p*-type doping with holes as conduction carriers. In comparison with single Li-doped Mg_2Si, double doping increased the carrier concentration to more than double.[13] In 2011, Sb doped $Mg_2Si_{0.5}Sn_{0.5}$ compound was synthesized and the peak power factor of the sample reached 3.2×10^{-3} $Wm^{-1}K^{-2}$ at 610 K with a maximum ZT >0.9, comparable to PbTe based thermoelectric materials.[14] In addition, Du *et al.* reported a maximum ZT of 0.85 was obtained at 700 K for $Mg_{2(1+x)}Si_{0.38}Sn_{0.6}Sb_{0.02}$ (x=0.1), and found that the carrier concentration and electrical conductivity were significantly enhanced by the Mg in the interstitial sites.[15] Moreover, Liu *et al.* also found high thermoelectric performance $Mg_{2(1+x)}Si_{0.45}Sn_{0.537}Sb_{0.013}$ (x=0.04-0.12) with a maximum ZT of 1.0 at 725 K for x=0.08 and a carrier concentration 1.9×10^{20} cm^{-3}.[16] Khan *et al.* reported that an even higher figure of merit (ZT) of 1.4 can be obtained at 800 K for multi-doped compound of $Mg_2Si_{0.55}Sn_{0.4}Ge_{0.05}$ doped with Bi.[17] Le-Quoc reported Hall effect measurements at room temperature on a thin film of Sb doped $Mg_2Si_{1-x}Sn_x$ (x=0.4, 0.5, 0.6) and showed that Sb acted as electrons donors but the carrier concentration increased non linearly with the Sb content. The electrical conductivity of the Sb doped films, however, is still low with a charge carriers concentration less than 10^{19} cm^{-3}.[18] In 2014, a significant enhancement of the thermoelectric figure of merit of Mg_2Si to 0.7 at 873 K was

a.Department of Physics and Engineering Physics, University of Saskatchewan, Saskatoon, SK S7N 5E2, Canada
b.Geophysical Laboratory, Carnegie Institution of Washington, Washington, DC 20015, USA
c.Canadian Light Source Inc, Saskatoon, SK S7N 2V3, Canada
d.Department of Applied Science, Faculty of Science, Okayama University of Science, Okayama, Japan
e.Department of Materials Science and Technology, Tokyo University of Science, Tokyo, Japan
f.The Institute for Solid State Physics, The University of Tokyo, Chiba, Japan
* Author to whom correspondence should be addressed: john.tse@usask.ca

achieved by double-doped with a combination of Bi, Pb, and Sb. It was observed that the addition of any two of the doping elements can increase the electrical conductivity due to the excess free electrons in the conduction band.[19] For example, Jiang *et al.* found the thermoelectric performance was improved by introducing three types of point defects, Sb dopants, Mg vacancies, and Mg interstitials, in $Mg_2Si_{0.4}Sn_{0.6-x}Sb_x$ samples.[20] Isoda *et al*. found the highest ZT value in a Al/Sb double-doped $Mg_2Si_{0.75}Sn_{0.25}$ of 0.94 at 850 K. Therefore, Sb is considered to be an effective dopant to increase the carrier concentration.[21] Previous studies have shown that double or multi-doping is a promising approach to further enhance the thermoelectric figure of merit (ZT) in Mg_2Si-based thermoelectric materials.

The objective of this paper is to characterize and to better understand the effect of multi-dopants on the host lattice of Mg_2Si crystal. For this purpose, Sb, Al, and Zn multi-doped Mg_2Si samples were synthesized by spark plasma sintering technique. The electrical transport properties were studied by mid-infrared reflectivity measurements. Since the reflectivity is related to the dielectric function, frequency dependent optical conductivity can be extracted from the analysis. Static (*dc*) conductivity is obtained by extrapolation to zero photon energy. In addition, electrical resistivity and Hall coefficient were also measured with conventional quasi-four-probe method. Thermoelectric properties of the multi-doped Mg_2Si samples were determined from the temperature dependency of the Seebeck coefficient (S), electrical conductivity (σ), and thermal conductivity (κ). The figure of merit (ZT) and power factor ($S^2\sigma\times T$) of Sb, Al, and Zn multi-doped Mg_2Si samples were then calculated.

The layout of the paper is as follow. First, details on the experimental procedure will be described. The diffraction patterns of multi-doped Mg_2Si are compared with pure Mg_2Si. This is followed by a discussion on the electrical properties extracted from mid-IR reflectivity and conventional quasi-four probe method. Finally, the thermoelectric properties were characterized from results on the temperature dependent of Seebeck coefficient (S), electrical conductivity (σ), and thermal conductivity (κ). The figure of merit (ZT) and power factor ($S^2\sigma\times T$) were calculated and discussed.

Experimental details

Synthesis and Sintering Process for Doped Mg_2Si Samples Preparation

Crystal growth of polycrystalline Mg_2Si was performed using an electric furnace by lowering the temperature from slightly beyond the melting point (1378 K) of Mg_2Si, and was initiated from stoichiometric melts with Mg : Si = 2 : 1. The starting materials, Mg, Si were placed in an alumina crucible under argon-hydrogen forming gas (0.08Mpa). Intentional impurities of antimony (Sb) and aluminium (Al), and an isoelectric impurity of zinc (Zn) were incorporated in order to increase the electronic carrier concentrations and phonon scattering. The Sb and Al dopants predominantly substitute to Si and Mg, respectively, which act as donors, and Zn is expected to show isoelectric characteristics at Mg site, *i.e*., no contribution to carrier generation but an influence over phonon behaviour, bringing about reduction in thermal conductivity. These donor and isoelectric dopants were incorporated during the all-molten synthesis process at 1378 K, and the resultant polycrystalline Mg_2Si was pulverized to powder with a size of 25~75μm, then placed into a graphite die and sintered by a plasma-activated sintering (PAS) technique using an ELENIX Ed-PAS-III-Es. The sintering was basically performed at 1123 K for 10 min. with a pressure of 40 MPa in an Ar (0.06 MPa) atmosphere and the sintering temperature and time were varied depending on the type of dopant that was used to obtain a dense material. The compositions of the samples were analyzed by electron-probe microanalysis (EPMA) using JEOL JXA-8900. The concentration of the dopant impurities in the samples was estimated by grow discharge mass spectrometry (GDMS) using V.G.Scientific VG-9000.

Powder X-ray Diffraction Measurement

Powder Mg_2Si from Alfa Products with a purity of 99.5%. Mg_2Si was doped with nominal 0.5 at. % of Sb, 0.5~1.0 at. % of Al, 0.5~1.0 at. % of Zn by the spark plasma sintering technique. The four materials studied were Mg_2Si with nominal at. % of Sb0.5% Al0.5% Zn0.5%, Sb0.5% Al1.0%, Sb0.5% Zn0.5%, and Sb0.5% Zn1.0%. Synchrotron X-ray diffraction experiments on the pure standard and doped Mg_2Si samples were performed at CMCF-II, Canadian Light Source (CLS), using synchrotron radiation (λ=0.68880 Å). The diffraction patterns were analyzed using the JANA 2006 software package with the lattice parameters determined by Le Bail fit.[22-23]

Mid-Infrared Reflectivity Measurement

Mid-infrared normal-incidence reflectance spectra on pure and Sb Zn Al multi-doped Mg_2Si samples were measured at the side-station of the U2A beamline, National Synchrotron Radiation Facility, Brookhaven National Laboratory. Mid-infrared spectra were recorded on a Bruker Vertex 80v FTIR spectrometer and a Hyperion 2000 IR microscope attached with a liquid nitrogen cooled HgCdTe detector. Powder samples were prepared and placed the 300 μm culet of a Sintek mini type IIa diamond anvil cell. After loading the sample the DAC is closed with hand compression to flatten the powder sample. After re-opening the DAC, one half of the flattened sample was removed leaving half of the clean diamond face exposed. In this way, the orientation of the sample surface and diamond support is ensured to be the same. This is critical for the conversion of the reflectance to absolute reflectivity. The procedure is as follow, the reflectance of diamond phase (I_d) and the sample (I_{sa}) were measured. The reflectance of the sample was then converted to absolute reflectivity by normalization to the reflectance of the diamond surface. From the known reflectivity of diamond, the reflectivity of sample-air interface (R_{sa}) was calculated as $R_{sa}= (I_{sa}/I_d)\times(I_d/I_0)$, where I_d/I_o is a constant of 0.185. All the

spectral data were collected at a resolution of 4 cm^{-1} and accumulated for 512 scans.

Frequency dependent optical conductivity was obtained by Kramers−Kronig (K−K) analysis of the reflectivity data by fitting with a variational K−K constrained dielectric function, implemented in the RefFIT code.[24,25] The frequency dependent optical conductivity was derived from the fit to a Drude-Lorentz (DL) model and the *dc* conductivity obtained from extrapolation to zero frequency.

Electrical Transport Properties and Thermoelectric Properties Measurements

Polycrystalline Mg_2Si fabricated by an all-molten synthesis method was used as the source material. The Sb, Al and Zn dopants were incorporated during a melt synthesis process at 1378 K, and the resultant polycrystalline Mg_2Si was pulverized to powder with a size of 25~75μm, then placed into a graphite die and sintered by a plasma-activated sintering (PAS) technique using an ELENIX Ed-PAS-III-Es. The sintering was performed at a pressure of 40 MPa in an Ar (0.06 MPa) atmosphere and the sintering temperature and time were varied depending on the type of dopant that was used to obtain a dense material. The temperature-dependent thermoelectric properties were measured using an ULVAC-RIKO ZEM2 to determine the Seebeck coefficient and the electrical resistivities, and an ULVAC-RIKO TC-7000H to determine the thermal conductivity over a temperature range from 300 K to 900 K. Electrical resistivity below room temperature was measured by the standard four-probe method in a commercial Quantum Design Physical Property Measurement System (PPMS) (1.8K T 400K, 0 H 70kOe). Hall effect was measured at fixed temperature by changing the magnetic from -5T to 5T.

Results and Discussion

High resolution synchrotron angle dispersive X-ray diffraction patterns of pure Mg_2Si, Mg_2Si doped with Sb0.5%Al0.5%Zn0.5%, Sb0.5%Al1.0%, Sb0.5%Zn0.5%, and Sb0.5%Zn1.0% were measured with photon of 18 KeV (λ=0.68880 Å) on the CMCF-II beamline Canadian Light Source Inc. at room temperature, (Fig. 1) The lattice constants were determined from full profile Le Bail fit to the diffraction patterns from 5° to 40° using the JANA 2006 package. The X-ray diffraction pattern of pure Mg_2Si can be indexed readily to the cubic anti-fluorite (CaF_2) structure with space group *Fm-3m*. In increasing diffraction angle, the miller indices (*hkl*) of the Bragg peaks are identified as (111), (200), (220), (311), (222), (400), (331), (420), (422), (511), (440), (531) and (600) reflections. The diffraction patterns of Mg_2Si doped with Sb, Zn and Al all share the same profile to pure Mg_2Si except the Bragg peaks have shifted noticeably to lower angles. The observation indicated that even with a small dopant concentration (0.5%~1.0%) the cubic lattice of Mg_2Si is expanded. Fig. 2 (a) and (b) summarize the experimental lattice parameters and unit cell volumes for pure Mg_2Si and doped Mg_2Si. The cubic cell parameter of pure Mg_2Si a= 6.2843(9) Å is increased to 6.3506(9) Å to 6.3634(9) Å by the addition of the dopants (Zn, Al, Sb). This can be rationalized as the atomic sizes of Zn, Al dopants are larger than Mg, and Sb, which replace the Si, also has a is bigger size We can conclude unequivocally that the cubic cells of all the doped samples are larger than pure Mg_2Si. The observations also lend support to the expectation that Al and Zn dopants will occupy the Mg sites, while Sb replaced Si in the Mg_2Si crystal structure. If this is the case, Al, Zn, and Sb doped Mg_2Si are an *n*-type semiconductors. As will be shown latter, this assignment is in agreement with the negative Hall coefficients.

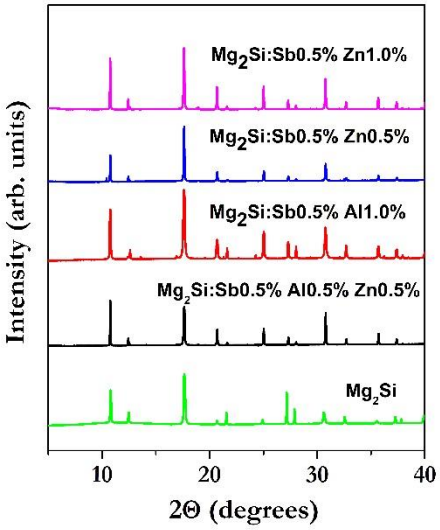

Fig. 1. Angle dispersive x-ray diffraction patterns of pure Mg_2Si and doped Mg_2Si measured at room temperature.

Further analysis of the lattice constants of the doped samples show, for instance, when compared with Mg_2Si: Sb0.5%Zn0.5%, the lattice constants of Mg_2Si: Sb0.5% and Zn1.0% is expanded, possibly due to the higher doping concentration of Zn. On the other hand, between Mg_2Si: Sb0.5%Zn1.0% and Mg_2Si: Sb0.5%Al1.0%, where the only difference is the doped element (*i.e.* Zn *vs*. Al). The lattice parameter in Mg_2Si: Sb0.5%Zn1.0% is slightly larger, as the size of Zn is larger than Al. In comparison, the lattice parameter of Mg_2Si: Sb0.5%Zn0.5% is comparable with Mg_2Si: Sb0.5%Al0.5%Zn0.5%, suggesting that Al has a weaker effect on the expansion of the crystal lattice, probably due to the similar atom sizes of Al and Mg atoms.

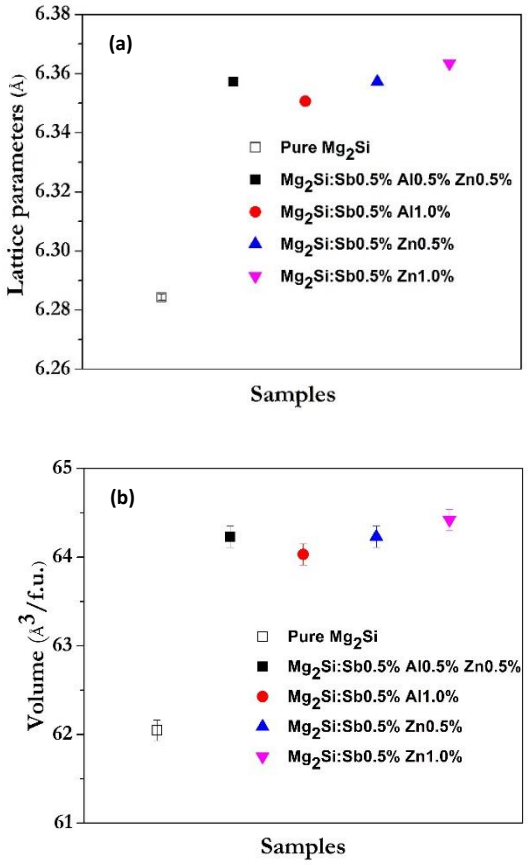

Fig. 2. (a) Lattice parameters of pure and doped Mg_2Si; (b) The volume per formula of pure and doped Mg_2Si.

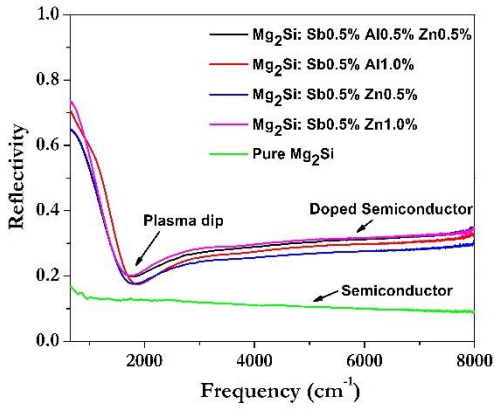

Fig. 3. Mid-infrared reflectivity spectra of pure and doped Mg_2Si.

Infrared reflectivity experiment can provide information on the electrical transport of a material. Mid-infrared reflectivity spectra were measured with an internal Globar radiation source (600 cm^{-1}-8000 cm^{-1}) installed at the U2A beamline on pure Mg_2Si and Mg_2Si multi-doped with Sn Zn and Al. The electronic transport properties of the doped samples were extracted. The experimental reflectivities for pure and mulit-doped Mg_2Si are compared in Fig. 3. The infrared reflectivity of all the doped Mg_2Si samples exhibit a Drude-like behavior at low frequency indicative of doped semiconductor. In comparison, the un-doped Mg_2Si sample does not have the free electron-like feature, indicating it is a semiconductor with a small band gap. This is to be expected as Mg_2Si is a semiconductor with a small indirect band gap of 0.6 eV.[27] In comparison to the flat and featureless reflectivity of pure Mg_2Si, the reflectivities of the multi-doped samples extrapolated to zero frequency are much higher. Note that a good conductor, such as copper or aluminum, has a reflectivity close to unity at zero frequency.

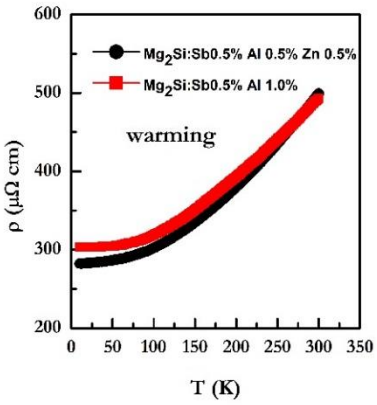

Fig. 4. Temperature dependent electrical resistivity of doped Mg_2Si by conventional quasi-four-probe method.

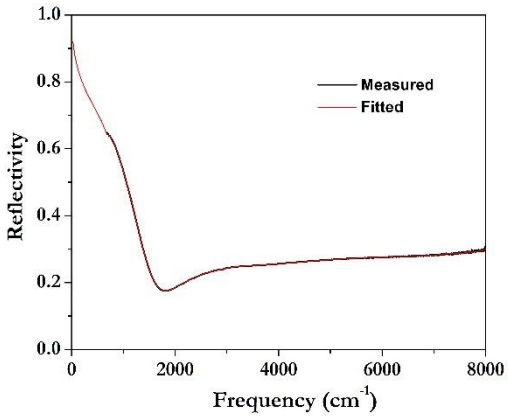

Fig. 5. A comparison of measured and fitted infrared reflectivity spectra of 0.5% Sb & 0.5% Zn doped Mg_2Si.

The Sb, Zn, Al-doped Mg_2Si samples show a common feature in the reflectivity curves around 1800 cm^{-1}. It is the appearance of a "dip" in the spectra. The minimum in the reflectivity is characteristic of a doped semiconductor and is known as the plasma reflection edge or plasma dip.[28] According to the simple Drude model, the energy at the energy minimum (plasma frequency ω_P) is related to the carrier concentration (N) and the effective mass (m^*), $\omega_P^2 = Ne^2/\varepsilon\varepsilon_0 m^*$ where ε is the dielectric constant of the material,

and ε_0 is the vacuum permittivity.[29] Therefore, the effective mass (m^*) of a doped semiconductor can be extracted from the plasma frequency (ω_P) provided the electron concentration (N) is known. Detail results will be reported, analyzed and discussed below.

The frequency dependence conductivity, the optical conductivity, can be obtained by performing a Kramers–Kronig (K–K) analysis on the reflectivity data.[25] The procedure is as follow, the optical conductivity obtained from a variational K-K transformation is fitted to a Drude-Lorentz (DL) model and the *dc* conductivity is estimated by extrapolation to zero frequency. A comparison illustrating the quality of the fit is shown in Fig, 5. In the figure, the raw and fitted infrared reflectivity spectra of 0.5% Sb&0.5% Zn doped Mg_2Si sample are compared. The *dc* conductivities of the doped samples obtained with this procedure are reported in Table I. The Mg_2Si: Sb0.5%Zn1.0% sample is found to have the highest *dc* conductivity of 767 S cm^{-1} and an extrapolated reflectivity of ~0.73 at zero frequency. The trend of the *dc* conductivities extracted from infrared reflectivity agree qualitatively with bulk electrical measurements.[26]

Table I. Summary of *dc* conductivity (σ_0) & carrier relaxation time (τ) of doped Mg_2Si.

Compound	σ_0 (S cm^{-1})	τ (s)
Mg_2Si: Sb0.5%Al0.5%Zn0.5%	507	3.72×10^{-14}
Mg_2Si: Sb0.5%Al1.0%	627	3.94×10^{-14}
Mg_2Si: Sb0.5% Zn0.5%	480	3.77×10^{-14}
Mg_2Si: Sb0.5%Zn1.0%	767	5.57×10^{-14}

The static *dc* conductivity increased dramatically from pure Mg_2Si, due to the larger concentration of free electrons in the conduction band by doping with Zn, Al, and Sb. From the free electron model, *dc* conductivity is proportional to the electron concentration (N), and scattering time (τ). The electron scattering time (τ) is a parameter in the Drude-Lorentz model and can be obtained from the fitting of the reflectivity data.[28] The fitted relaxation times of doped Mg_2Si samples are tabulated in Table I. The derived relaxation times of *ca*. 10^{-14} sec. is consistent with other doped semiconductors. The electron concentration (N) in a doped semiconductor is the density of the mobile electrons or holes, (n- or p- doped). Since the host crystal Mg_2Si is the same for all samples, the *dc* conductivity depends only on the nature of the dopants. The dramatic enhancement of the *dc* conductivity by the dopants is due to the occupation of the free electron-like conduction bands. In spite of the simplicity of the Drude-Lorentz model and the neglect of low frequency (<600 cm^{-1}) absorption which is not accessible by mid-infrared radiation, the results indicate that the *dc* conductivity can be improved by addition of the (Zn Al Sb) dopants.

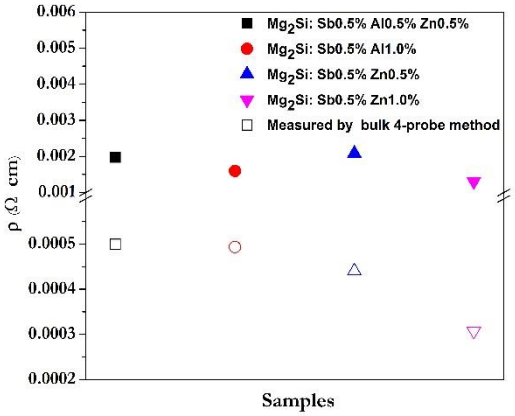

Fig. 6. A comparison of electrical resistivity (ρ) extracted from infrared reflectivity spectra and measured by quasi-four-probe method.

Although the trend of increasing electrical resistivity and reflectivity is the same from IR reflectivities and four-probe conductivity measurements, the comparison of the absolute magnitude is less satisfactory. (Fig. 6) The *dc* conductivities derived from infrared reflectivity has the same order of magnitude as the bulk measurements, but are approximately four times smaller. One contributing factor may be the infrared beam only surveyed a very small region (20×20 μm^2) within a couple of microns into the sample surface. This is different from the quasi-four-probe conductivity method which is a bulk sensitive technique. At the sample surface the atom density is less than the bulk and the chemical bonding in the surface is also stronger.[30,31] Therefore, there are less free electrons near the sample surface thus reducing the electrical conductivity. Although plausible, this effect cannot satisfactory explain the discrepancy observed here. Since the *dc* conductivity was obtained from the extrapolation of the frequency dependent conductivity to zero frequency, it is not certain if the omission of reflectivity at very low energy (*i.e.* < 600 cm^{-1}) may have an effect. From past experience, we expect the *dc* conductivity derived from an IR measurement should agree within an order of the magnitude of the value obtained from the bulk technique.[10,32] We found no systematic error in the experiment and on the treatment of the data. In a previous study, we have also compared the *dc* conductivity derived from IR reflectivities to bulk measurements on doped Mg_2Si and the agreements were favorable.[10] We suspect the most likely source of the disagreement may be related to a precise knowledge on the concentration of the dopants. The doped samples used in this study were synthesized by plasma spark sintering method. It is very difficult to control the precise stoichiometry. Another possible source of the discrepancy may be due to non-uniform distribution of dopants in the sample. In a study of Sb and Bi doped-Mg_2Si, it was found by high resolution transmission microscopy (TEM) that due to the limited solubility excess Sb and Bi atoms are present in the grain boundaries that may enhance the conductivity of the bulk sample.[10] In comparison, IR measurements only examine

a very small spot of *ca*. 20×20 μm² of the sample so this may produce different results. Finally, the formation of a thin oxide layer on the surface may also contribute to the lower conductivity derived from the IR experiments. A careful characterization of both samples is critical to resolve the discrepancy.

The bulk electrical transport properties of the Zn Al Sb multi-doped Mg_2Si samples were determined by temperature dependent electrical resistivity and Hall coefficient with the quasi-four-probe method. The temperature dependent electrical resistivities (ρ) of doped Mg_2Si samples (Fig.4) were measured with a current of 3 mA and sectional areas between 1.05×0.78 mm² ~ 1.45×1.01 mm². It is found that the electrical resistivity of Mg_2Si: Sb0.5%Al1.0% increased from 300 μΩ cm to 500 μΩ cm from 10 K to 300 K. At 300 K, the electrical resistivity in Mg_2Si: Sb0.5%Zn1.0% is smaller than the other doped samples of 430~500 μΩ cm. The results suggest that there are more free electrons in the conduction band of the other samples leading to higher electrical conductivity. Comparing Mg_2Si: Sb0.5%Zn0.5% and Mg_2Si: Sb0.5%Zn1.0%, the electrical resistivities were found to decrease with concentration of the Zn dopant. Since the concentrations of Sb were the same in these two samples and the Zn atoms were expected to occupy the Mg sites, this conductivity trend suggests there are more mobile electrons in the conduction band with more Zn dopants.

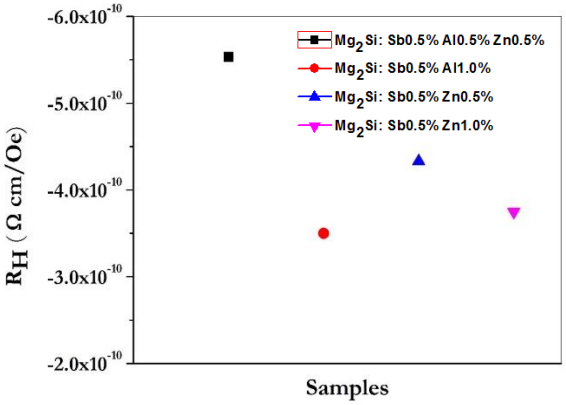

Fig. 7. Hall coefficients (R_H) of doped Mg_2Si samples were measured by quasi-four-probe method.

The measured Hall coefficients (R_H) of Zn, Al, Sb-doped Mg_2Si samples are shown in Fig. 7. The negative and almost constant Hall coefficients show the multi-doped Mg_2Si materials are *n*-type doped semiconductors. Using the equation $N=1/(eR_H)$, (where *e* is the electron charge, and R_H is the Hall coefficient) the electron concentrations (*N*) were calculated and show in Table II. Possibly, Mg_2Si: Sb0.5%Al1.0% has the largest electron concentration (*N*) of 1.78×10^{20} cm^{-3}, due to the high doping concentration. The electron concentration (*N*) of the multi-doped Mg_2Si samples of *ca*.10^{20} cm^{-3} are in reasonable agreement with that estimated from the free electron model. Therefore doped-Mg_2Si are doped semiconductors.[28] The results are supported by the low plasma frequencies of the doped samples. The low plasma frequencies observed in the IR region is also indicative of a doped semiconductor.

Table II. Summary of electron concentration (*N*) calculated from Hall coefficient (R_H) of doped Mg_2Si.

Compound	R_H (cm^3/C)	*N* (cm^{-3})
Mg_2Si: Sb0.5%Al0.5%Zn0.5%	-5.53×10^{-2}	1.17 ×10^{20}
Mg_2Si: Sb0.5%Al1.0%	-3.50×10^{-2}	1.78 ×10^{20}
Mg_2Si: Sb0.5% Zn0.5%	-4.33×10^{-2}	1.44 ×10^{20}
Mg_2Si: Sb0.5% Zn1.0%	-3.75×10	1.67×10^{20}

Table III. Summary of effective mass (m*) of doped Mg_2Si calculated from the plasma frequency (ω_p) within the infrared reflectivity.

Compound	ω_p (cm^{-1})	m^*/m_e
Mg_2Si: Sb0.5%Al0.5%Zn0.5%	1791	0.255
Mg_2Si: Sb0.5%Al1.0%	1899	0.346
Mg_2Si: Sb0.5% Zn0.5%	1788	0.316
Mg_2Si: Sb0.5%Zn1.0%	1798	0.361

The effective mass can be calculated from the plasma frequency observed in the infrared reflectivity and the electron concentration from the Hall coefficient.[33] The plasma frequency ω_P is related to the electron concentration (*N*) and the effective mass (m^*) by $\omega_P^2 = Ne^2/\varepsilon\varepsilon_0 m^*$, where ε is the dielectric constant of the material, and ε_0 is the vacuum permittivity.[34] Therefore, the effective mass (m^*) is inversely proportional to the square of plasma frequency (ω_P). Assuming a constant optical dielectric constant (ε) of 12.82 for doped Mg_2Si samples,[35] the effective masses were calculated for all the doped Mg_2Si samples studied. As shown in Table III, the effective masses of doped Mg_2Si samples are between $0.255m_e$ and $0.361m_e$, where m_e is the mass of a free electron. The light effective masses found in this work are comparable with previous measurements listed in Table IV. Electrons with lighter effective mass are easier move in the conduction band and therefore contribute to a higher electrical conductivity. The light effective masses *i.e*. $0.255m_e$ to $0.361m_e$ of doped Mg_2Si show occupation of free-electron-like conduction band by the excess electron donated by the dopants.[11]

Table IV. Summary of the effective masses for pure and *n*-doped Mg_2Si reported in the literature.

Pure Mg_2Si	$0.4m_e$[36]	$0.5m_e$[37]	
$Mg_2Si_{0.98}Sb_{0.02}$	$1m_e$[36]	$1.06m_e$[10]	$1.1m_e$[38]
$Mg_2Si_{0.98}Bi_{0.02}$	$0.62m_e$[10]	$0.5m_e$[39]	

To define the thermoelectric properties of doped Mg_2Si samples, the temperature dependent electrical conductivity (σ), Seebeck coefficient (S), power factor ($S^2\sigma T$), thermal conductivity (κ) were measured up to 900 K, and the

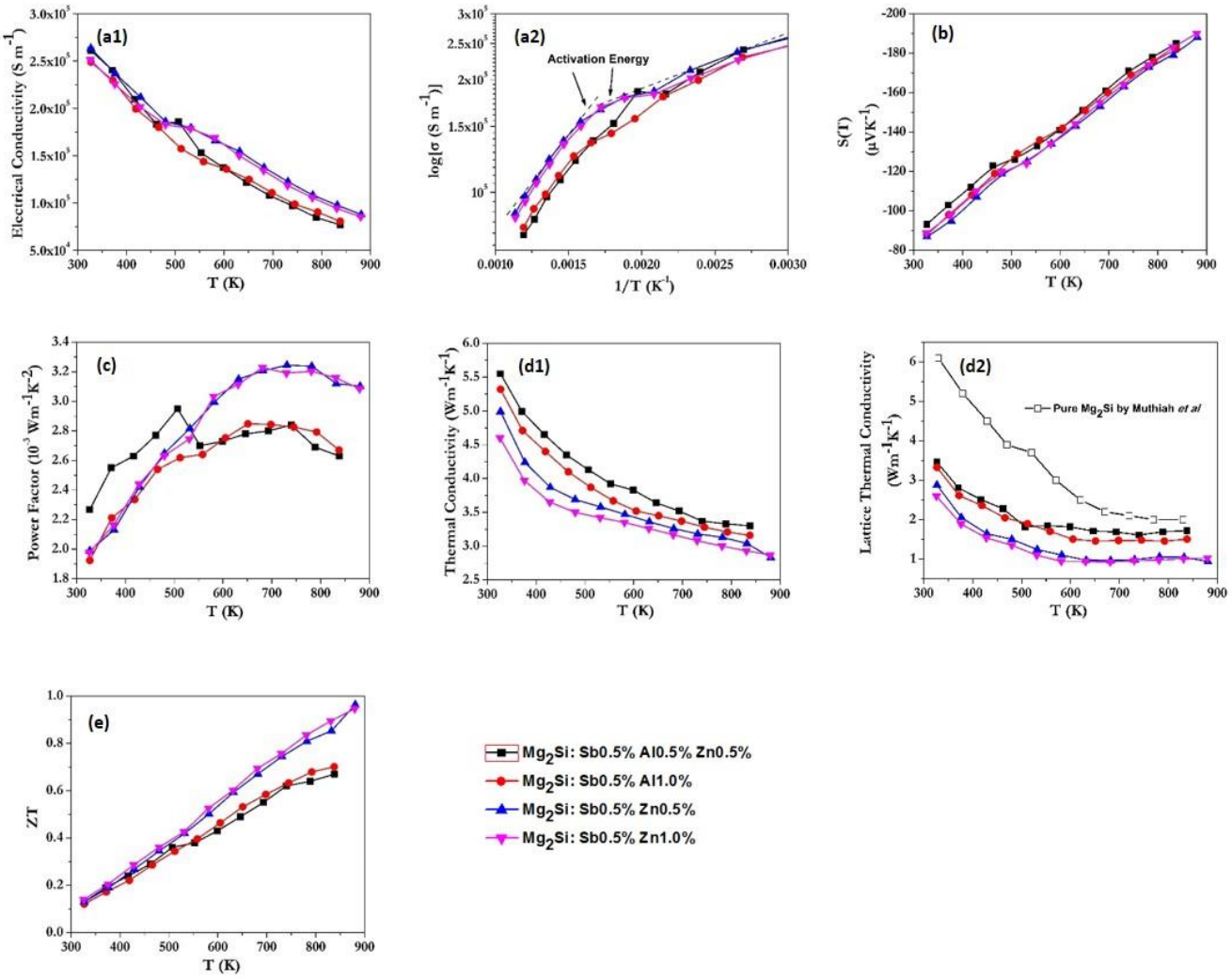

Fig. 8 Temperature dependent (a1)&(a2) electrical conductivity, (b) Seebeck coefficient, (c) Power factor, (d1)&(d2) Thermal conductivity & Lattice thermal conductivity, and (e) Figure of merit (ZT).

corresponding figure of merit (ZT) were calculated. As show in Fig. 8 (a)-(e), the electrical conductivity of doped Mg_2Si decrease from 2.5×10^5 S m^{-1} to 0.8×10^5 S m^{-1} when the temperature is raised from 300 K to 900 K. The highest electrical conductivity obtained in the present study is 2.6×10^5 S m^{-1} for Mg_2Si: Sb0.5%Zn0.5% at room temperature (300 K). The electrical conductivity of double or multi-doped Mg_2Si is substantially larger when compared to the un-doped Mg_2Si (15 S m^{-1}).[19] A small amount of dopants (0.5%~1.0%) is found to have a dramatic impact on the electrical conductivity. In all four multi-doped Mg_2Si samples, an increase of electrical conductivity were observed. The conductivities derived from infrared reflectivities show the correct trend expected from the free electron model. (*i.e.* the conductivity of Mg_2Si: Sb0.5%Al1.0% is higher than Mg_2Si: Sb0.5%Zn0.5%) as Al donates more electrons than Zn when substituted the Mg sites. The reverse was apparently observed in the bulk measurements. (Fig. 8) This discrepancy may be attributed to non-homogeneity of the dopants. Moreover, the free electron model is only a simplification and the true conductivity also depends on the effective mass of the conducting electron, which is related to the dispersive of the occupied conduction band. If the bulk measurements are more representative of the property of the sample, we may speculate that the effective mass of the conducting electrons in Mg_2Si: Sb0.5%Al1.0% is heavier. In fact, as shown in Table III, the derived effective mass of the electron in Mg_2Si: Sb0.5%Al1.0% of $0.346m_e$ is heavier than Mg_2Si: Sb0.5%Zn0.5% of $0.316m_e$. It is interesting to note that there is a distinctive discontinuity in the Mg_2Si: Sb0.5%Al0.5%Zn0.5% at 450K~500 which will be discussed below (*vide supra*).

From the temperature dependence of the electrical conductivity, the activation energy of the doped Mg_2Si samples in the temperature range, 300 K-800 K, can be defined from the Arrhenius equation $\rho = \rho_0 \exp(-E_t/kT)$, where ρ is the electrical resistivity, ρ_0 is the high temperature resistivity, E_t is the activation energy, k is the Boltzmann constant, and T is the temperature. The value of E_t can be determined from the plot of ln(ρ) vs. (1/T). As shown in Fig. 8 (a1)&(a2), between 450 K and 550 K, the trend of Mg_2Si: Sb0.5%Al0.5%Zn0.5% does not

follow the relationship with increasing the temperature as the others. The sudden change of activation energy (E_t) further implies that a possible structure change has occurred.[40] Since the high temperature crystal structure is still unknown, a definitive will characterization require a high temperature X-ray diffraction powder diffraction study.

Throughout the temperature range studied, the Seebeck coefficients (S) of Sb, Al, Zn multi-doped Mg_2Si samples are negative confirming they are *n*-doped semiconductors, in agreement with the Hall coefficients. The values for the temperature dependent Seebeck coefficient (S) are quite similar for all doped samples, suggesting the dopants play a similar role to enhance the Seebeck coefficient. The Seebeck coefficient increased from -90 μVK^{-1} to -190 μVK^{-1} with increasing temperature and reached a maximum value at 900 K. The Seebeck coefficients for the doped Mg_2Si samples are comparable with the previously reported Bi, Pb, and Sb double-doped Mg_2Si.[19] For un-doped Mg_2Si sample, the Seebeck coefficient increased initially with increasing temperature and reach the maximum value at 450 K. Above 450 K, the value of Seebeck coefficient started to decrease.

Fig. 8 (c) shows the calculated power factor ($S^2\sigma\times T$) of doped Mg_2Si samples. The general trend of the calculated temperature dependent power factor increased initially and peaked at ~750 K then drop with further increase of the temperature. The maximum power factor is due to the effect that Seebeck coefficient (S) increases faster than decrease in the electrical conductivity (σ). At further increase in temperature, the power factor decreases gradually, as the electrical conductivity (σ) becomes more important to power factor than the Seebeck coefficient (S). A peak power factor of 2.9×10^{-3} $Wm^{-1}K^{-2}$ was found at 500 K in Mg_2Si: Sb0.5%Al0.5%Zn0.5%, close to the possible structural phase transition. Fig. 8 (d1) shows the temperature dependent thermal conductivity of the doped Mg_2Si samples. The general trend of the thermal conductivities is to decrease with increasing temperature. This is obviously due to increase in phonon scatterings at higher temperature. At 310 K, the thermal conductivity of Mg_2Si: Sb0.5%Al0.5%Zn0.5% (5.6 $Wm^{-1}K^{-1}$) is higher than other doped Mg_2Si samples. However, all the thermal conductivities of doped Mg_2Si samples are lower than un-doped Mg_2Si (6.2 $Wm^{-1}K^{-1}$). Phonon scatterings become more efficient at the presence of heavier dopants in the lattice. Total thermal conductivities (κ_{total}) can be separated into two contributions the lattice (κ_{ph}) and the electronic (κ_{el}) conductivity. The electronic conductivity (κ_{el}) can be estimated by the Wiedemann-Franz law, where $\kappa_{el}= L\sigma T$ (the Lorentz number (L) is 2.45×10^{-8} V^2/K^2).[41] The lattice thermal conductivity (κ_{ph}) can then be estimated by subtracting the electronic thermal conductivity (κ_{el}) from the total thermal conductivity (κ_{total}). Considering the major contribution of lattice thermal conductivity (κ_{ph}) to the total thermal conductivity (κ_{total}), Fig. 8 (d2) shows the temperature dependent of the lattice thermal conductivity (κ_{ph}). Compared to Al, the heavier Zn dopants are better phonon scatters, leading to lower lattice thermal conductivity. The observed trend,Mg_2Si:Sb0.5%Al0.5%Zn0.5%>Mg_2Si:Sb0.5%Al1.0%>Mg_2Si : Sb0.5%Zn0.5%> Mg_2Si: Sb0.5%Zn1.0%) is expected. Similarly, the lattice thermal conductivity of Mg2Si: Sb0.5%Zn0.5% and Mg2Si: Sb0.5%Zn1.0% samples are lower than others because the phonon scatterings become more efficient at the present of heavier Zn dopants. The only exception is Mg_2Si: Sb0.5%Al0.5%Zn0.5% which has a higher thermal conductivity than Mg_2Si: Sb0.5%Al1.0%. At this moment, we cannot provide a satisfactory explanation for this observation. Using the information obtained above, the temperature dependent figure of merits (ZT) were calculated. (Fig. 8 (e)) For each doped-Mg_2Si sample, ZT increased significantly with increasing temperature. A maximum ZT of 0.964 is found in Sb0.5%Zn0.5% doped Mg_2Si at 880 K.

Conclusions

The structural information of Sb Al Zn multi-doped Mg_2Si powder samples synthesized from spark plasma sintering have been investigated by angle dispersive synchrotron radiation X-ray diffraction, infrared reflectivity, electrical and thermal conductivity measurements. The small concentration of dopant (0.5%~1.0%) did not alter the cubic crystal structure of the host Mg_2Si, but expanded the crystal lattice noticeably. The electrical transport properties were characterized by mid-IR reflectivity and quasi-four probe measurements. Infrared reflectivity shows doped semiconductor character for all the samples at room temperature. The *dc* conductivities calculated from the analysis of the infrared reflectivity spectra employing the Drude-Lorentz model are in qualitative agreement with the conventional bulk four-probe measurements although the absolute values obtained from IR reflectivities are consistently lower. The electron concentrations (*N*) were determined from the Hall coefficients and plasma frequencies (ω_P) of the infrared reflectivities. The multi-doped Mg_2Si are within the order 10^{20} cm^{-3}, suggesting that all doped-Mg_2Si are doped semiconductors. The effective masses ranged from $0.255m_e$ to $0.361m_e$ showing different dopants have slightly effect on the band structure of Mg_2Si. A maximum thermoelectric figure of merit (ZT) of 0.964 was achieved in Sb0.5%Zn0.5% doped Mg_2Si sample at 880 K. The present study provides new results and insight on thermoelectric and electrical transport properties of Sb Al Zn multi-doped Mg_2Si from 300 K to 900 K. The information presented here may help to further enhance the performance of Mg_2Si-based thermoelectric materials.

Acknowledgements

Synchrotron work at the Canadian Light Source was made possible by support from NSERC, NRC, CIHR, and the University of Saskatchewan. The use of U2A beamline was supported by COMPRES under NSF Cooperative Agreement EAR 11-57758 and CDAC (DE-FC03 03N00144). The National Synchrotron Light Source, Brookhaven National Laboratory, was supported by the U.S. Department of Energy, Office of Science, Office of Basic Energy Sciences under Contract No. DE-AC02-98CH10886. The sample preparation and thermoelectric

measurements ware partly supported by a Grant-in-Aid for Research (A) by the Japanese Ministry of Education, Science, Sports, and Culture. The electrical resistivity measurement was supported by JSPS KAKENHI Grant Number 15F15023. JZ and JST thank AUTO21 for a research grant.

Notes and references

1 T. Sakamoto, T. Iida, S. Kurosaki, K. Yano, H. Taguchi, K. Nishio, and Y. Takanashi, *Journal of Electronic Materials*, 2011, **40**, 629-634.
2 S. Battiston, S. Fiameni, M. Saleemi, S. Boldrini, A. Famengo, F. Agresti, M. Stingaciu, M. S.Toprak, M. Fabrizio, and S. Barison, *Journal of Electronic Materials*, 2013, **42**, 1956-1959.
3 T. Sakamoto, T. Iida, A. Matsumoto, Y. Honda, T. Nemoto, J. Sato, T. Nakajima, H. Taguchi, and Y. Takanashi, *Journal of Electronic Materials*, 2010, **39**, 1708-1713.
4 S. You, K. Park, I. Kim, S. Choi, W. Seo, and S. Kim, *Journal of Electronic Materials*, 2011, **41**, 1675-1679.
5 J. Tani and H. Kido, *Intermetallics*, 2008, **16**, 418-423.
6 N. Wang, H. Chen, H. He, W. Norimatsu, M. Kusunoki, and K. Koumoto, *Scientific Reports*, 2013, **3**, 3449.
7 Q. Chen, Q. Xie, F. Zhao, D. Cui, and X. Li, *IEEE Computer Society*, 2009, **22**, 338-341.
8 G. J. Snyder, and E. S. Toberer, *Nature Materials*, 2008, **7**, 105-114.
9 G. H. Kim, L. Shao, K. Zhang, and K. P. Pipe, *Nature Materials*, 2013, **12**, 719-723.
10 N. Farahi, M. VanZant, J. Zhao, J. S. Tse, S. Prabhudev, G. A. Botton, J. R. Salvador, F. Borondics, Z. Liu and H. Kleinke, *Dalton Transactions*, 2014, **43**, 14983.
11 M. Akasaka, T. Iida, A. Matsumoto, K. Yamanaka, Y. Takanashi, T. Imai, and N. Hamada, *Journal of Applied Physics*, 2008, **104**, 013703.
12 Y. Isoda, S. Tada, T. Nagai, H. Fujiu, and Y. Shinohara, *Materials Transactions*, 2010, **51**, 868-871.
13 Y. Isoda, S. Tada, T. Nagai, H. Fujiu, and Y. Shinohara, *Journal of Electronic Materials*, 2010, **39**, 1531.
14 H. Gao, T. Zhu, X. Liu, L. Chen, and X. Zhao, *Journal of Materials Chemistry*, 2011, **21**, 5933.
15 Z. Du, T. Zhu, Y. Chen, J. He, H. Gao, G. Jiang, T. M. Tritt, and X. Zhao, *Journal of Materials Chemistry*, 2012, **22**, 6838.
16 X. Liu, T. Zhu, H. Wang, L. Hu, H. Xie, G. Jiang, G. J. Snyder, and X. Zhao, *Advanced Energy Materials*, 2013, **3**, 1238.
17 A. U. Khan, N. Vlachos, and Th. Kyratsi, *Scripta Materialia*, 2013, **69**, 606-609.
18 H. Le-Quoc, S. Bechu, S. Populoh, A. Weidenkaff, and A. Lacoste, *Journal of Alloys and Compounds*, 2013, **546**, 138-144.
19 S. Muthiah, B. Sivaiah, B. Gahtori, K. Tyagi, A. K. Srivastava, B. D. Pathak, A. Dhar, and R. C. Budhani, *Journal of Electronic Materials*, 2014, **43**, 2035.
20 G. Jiang, J. He, T. Zhu, C. Fu, X. Liu, L. Hu, and X. Zhao, *Advanced Functional Materials*, 2014, **24**, 3776.
21 Y. Isoda, M. Held, S. Tada, and Y. Shinohara, *Journal of Electronic Materials*, 2014, **43**, 2053.
22 V. Petricek, M. Dusek, and L. Palatinus, *Kristallogr.*, 2014, **229**, 345-352.
23 A. Le Bail, H. Duroy, and J. L. Fourquet, *Materials Research Bulletin*, 1988, **23**, 447-452.
24 R. L. Kronig, *Journal of the Optical Society of America and Review of Scientific Instruments*, 1926, **12**, 547-557.
25 A. B. Kuzmenko, *Review of Scientific Instruments*, 2005, **76**, 083108.
26 N. V. Morozova, S. V. Ovsyannikov, I. V. Korobeinikov, A. E. Karkin, K. Takarabe, Y. Mori, S. Nakamura, and V. V. Shchennikov, *Journal of Applied Physics*, 2014, **115**, 213705.
27 M. Y. Au-Yang, and M. L. Cohen, *Physical Review*, 1969, **178**, 1358.
28 M. Fox, *Optical properties of solids, 2nd edition, Oxford University Press*, 2010.
29 N. Farahi, S. Prahudev, G. A. Botton, J. Zhao, J. S. Tse, Z. Liu, J. R. Salvador, and H. Kleinke, *Journal of Alloys and Compounds*, 2015, **644**, 249-255.
30 D. M. Larson, K. H. Downing, and R. M. Glaeser, *Journal of Structural Biology*, 2011, **174**, 420.
31 S. Mafe, J. A. Manzanares, and P. Ramirez, *Physical Chemistry Chemical Physics*, 2003, **5**, 376.
32 J. W. L. Wong, A. Mailman, K. Lekin, S. M. Winter, W. Yong, J. Zhao, S. V. Garimella, J. S. John, R. A. Secco, S. Desgreniers, Y. Ohishi, F. Borondics, and R. T. Oakley, *Journal of The American Chemical Society*, 2014, **136**, 1070.
33 P. Perlin, E. Litwin-Staszewska, B. Suchanek, W. Knap, J. Camassel, T. Suski, R. Piotrzkowski, I. Grzegory, S. Porowski, E. Kaminska, and J. C. Chervin, *Applied Physics Letter*, 1996, **68**, 1114.
34 P. E. Blöchl, *Physical Review B*, 1994, **50**, 17953.
35 D. McWilliams, and D. W. Lynch, *Letters to The Editor*, 1962, **53**, 298.
36 Q. Zhang, *Rare Metal Materials and Engineering*, 2009, **38**, 166.
37 V. K. Zaitsev, M. I. Fedorov, E. A. Gurieva, I. S. Eremin, P. P. Konstantinov, A. Y. Samumin, and M. V. Vedernikov, *Phys. Rev. B: Condens. Matter*, 2006, **74**, 045207.
38 S. K. Bux, M. T. Yeung, E. S. Toberer, G. J. Snyder, R. B. Kaner, and J. P. Fleurial, *J. Mater. Chem.*, 2011, **21**, 12259-12266.
39 G. S. Nolas, D. Wang, and M. Beekman, *Phys. Rev. B: Condens. Matter*, 2007, **76**, 235204.
40 W. Ren, Y. Han, C. Liu, N. Su, Y. Li, B. Ma, Y. Ma, and C. Gao, *Solid State Communications*, 2012, **152**, 440-442.
41 C. Kittel, *Introduction to Solid State Physics, 8th edition, NJ:Wiley*, 2005.

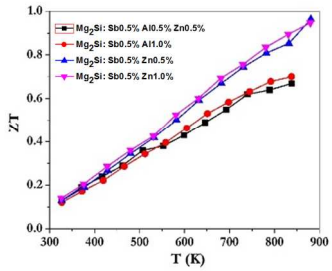

A maximum ZT of 0.964 was found in Sb0.5%Zn0.5% doped Mg_2Si, which is comparable to the PbTe based thermoelectric materials.